

Shape Features Extraction Using a Partial Differential Equation

TAKAYUKI YAMADA, Kyoto University, JAPAN

This paper presents a unified method for extraction of geometrical shape features in binary image data using a linear partial differential equation (PDE). The PDE and functions are formulated to extract geometrical shape features, which are thickness, shape orientation and skeleton, all at once. The main advantages of the proposed method are it is free of any computation with respect to distance, it has no topological constraint of target image data and surfaces do not have to be distinguished to inside or outside. A one dimensional analytical solution is provided to validate the proposed method. Additionally, two- and three-dimensional numerical examples are shown to confirm the validity and usefulness of the proposed method.

CCS Concepts: • **Computing methodologies** → **Shape analysis**; *Image processing*; • **Mathematics of computing** → *Partial differential equations*;

Additional Key Words and Phrases: Shape features, Local thickness, Shape orientation, Skeleton, Distance computation free

ACM Reference Format:

Takayuki Yamada. 2018. Shape Features Extraction Using a Partial Differential Equation. *ACM Trans. Graph.* 0, 0, Article 0 (June 2018), 11 pages. https://doi.org/0000001.0000001_2

1 INTRODUCTION

The development of remarkable image analysis technology in recent years has significantly contributed to solving many problems in various fields such as materials science [Yamashita et al. 2014], mechanical engineering [Benko et al. 2001], biomechanics [Sera et al. 2003; Zhenjiang 2000] and medicine [Hildebrand and Ruegsegger 1997; Hutton et al. 2008]. For example, extraction of skeletons from image data such as computed tomography (CT) and magnetic resonance imaging (MRI) has contributed to the understanding of internal structure in medical diagnosis support. In particular, the estimated local thickness is one significant measure for disease propagation. In reverse engineering of mechanical products [Fujimori and Suzuki 2005], geometrical shape feature extraction such as curvature and edge information from measured shape data such as X-ray CT images is an important analysis technique to obtain a design solution with high performance in a short development period. The shape feature extractions are used in a variety of computer vision and image processing tasks.

This paper presents a unified method for extraction of geometrical features in image data by using a partial differential equation (PDE). In the following section, related works of the shape feature extraction and PDE based image processing are briefly discussed. Second, the basic concept and overview of my proposed method are discussed based on the comparison between related works and the proposed method. Next, the PDE for geometrical shape feature extraction is formulated. The shape feature functions for thickness,

shape orientation and skeleton are formulated based on the proposed PDE. That is, these geometrical features are represented as a function of the solution of PDE. Additionally, a numerical algorithm for the proposed method is provided based on the finite element method. In Section 6, the validity of the proposed method is discussed based on a one dimensional analytical solution. Finally, to confirm the validity and utility of the proposed method, several numerical examples are provided for both two- and three- dimensional cases.

2 RELATED WORKS

Tensor scale is a measure of shape feature, which represents thickness, orientation and anisotropy [Andaló et al. 2010; Saha 2005]. The measure defines the parameters of the largest ellipse within the target domain at each pixel point. Although the measure represents several geometrical features all at once as with my proposed method, high computational cost is required because the Euclidean distance is computed for each point. Additionally, related works for each shape feature are briefly discussed as follows:

Thickness: One significant application of thickness extraction is bone thickness [Liu et al. 2014; Saha and Wehrli 2004]. The local thickness defined in [Hildebrand and Ruegsegger 1997] is estimated based on the fuzzy distance transformation [Saha et al. 2002] in these methods. The basic concept is sampling the depth values at axial voxels, which are computed by skeletonization techniques [Arcelli et al. 2011; Saha et al. 1997].

Another challenging application of measuring thickness is estimation of the cortical thickness of the human brain from MRI data [Clarkson et al. 2011; Hutton et al. 2008]. The method is classified to surface-based, voxel-based and its hybrid methods. In these methods, the image is separated into three domains, which are grey matter, white matter and cerebrospinal fluid. As discussed in [Clarkson et al. 2011], the surface-based method [Davatzikos and Bryan 1996] uses a generated mesh on one side surface. Next, the mesh is deformed to fit the pair surface under topological constraint. In general, the computation of the advection requires high computational cost to ensure the topology [Han et al. 2004].

On the other hand, the voxel-based methods are separated to morphological, line integral, diffeomorphic registration and Laplacian based methods. The morphological method [Lohmann et al. 2003] divides each voxel into inner and outer domains. The thickness is computed using the Euclidean distance transformation. In the line integral based approaches [Aganj et al. 2009; Scott et al. 2009], every line integral centered at each point is computed and the minimum value is defined as thickness. The basic concept of the diffeomorphic registration based approach [Das et al. 2009] is also computation of surface deformation. Jones et al. [Jones et al. 2000] proposed the Laplacian based approach. In the method, two surfaces consisting of target shape are considered. It is assumed that the surfaces are topologically equivalent to a sphere. The Laplace

Author's address: Takayuki Yamada, Kyoto University, C3, Kyoto-Daigaku-Katsura, Nishikyo-Ku, Kyoto, 615-8504, JAPAN, takayuki@me.kyoto-u.ac.jp.

© 2018 Association for Computing Machinery.

This is the author's version of the work. It is posted here for your personal use. Not for redistribution. The definitive Version of Record was published in *ACM Transactions on Graphics*, https://doi.org/0000001.0000001_2.

equation is considered in the domain surrounded by the two surfaces, which are imposed Dirichlet boundary conditions with different constant values. The thickness between these surfaces is defined as length along with the normal direction of the iso-surface of the potential field. Based on this approach, Yezzi et al. [Yezzi and Prince 2001, 2003] proposed the Eulerian approach to directly compute the thickness along with the normal direction. The hybrid Eulerian-Lagrangian approaches are also proposed [Acosta et al. 2009; Rocha et al. 2005]. The multiple Laplace equation is used for time dependent estimation problem [Cardoso et al. 2011]. The main advantage of the PDE approaches is that thickness is uniquely defined at any points. However, the basic idea is restricted under the topological constraint. Furthermore, the inner and outer subsurfaces have to be distinguished.

I remark that the proposed method is similar to the Laplacian based approach. However, the idea is applicable to not only voxel-based data but also surface-based data, because the proposed PDE can be easily solved by the boundary element method. Additionally, the proposed method essentially overcomes the topological problems and has the advantage that there is no need to divide surfaces into the inner and outer surface. Furthermore, the proposed PDE is well-posed. That is, the solution is uniquely computed and can be computed numerically stable.

Skeleton: The applications of skeleton [Blum and Nagel 1978; Montanari 1968] are found in a broad range of areas, such as medical science, animation and reverse engineering. As discussed in [Cornea et al. 2007], these methods are categorized to topological thinning methods [Palágyi and Kuba 1998; Saha et al. 1997], methods using a distance field [Arcelli et al. 2011; Bitter et al. 2001], geometric methods [Amenta et al. 2001] and methods using the generalized potential field model [Abdel-Hamid and Yang 1994]. The proposed method is closest to the generalized potential field model [Ahuja and Chuang 1997; Grigorishin et al. 1998]. The basic concept of generalized potential field model is considering a fictitious electro static potential field with sources on the surface. The main advantage of the method is that the methods provide relatively good results. However, high computational cost is required, because the Newton potential field is computed by superposition at each point. Additionally, these algorithms do not consider numerical stability in the mathematical point of view. Several approaches are proposed to overcome problems such as connectivity and robustness in recent years. For instance, the erosion thickness approach gives a robust and connected skeleton [Yan et al. 2016].

Additionally, the PDE based approaches are also used in widely related fields as follows:

Image Processing: The PDE of elliptic type is also extensively used in the image processing field. Poisson image editing [Pérez et al. 2003] is a method of image editing by solving the Poisson equation. The basic idea is preserving the gradient of a source image for seamless image editing. The pixels with high gradient are extracted by using the Poisson equation. Poisson matching [Sun et al. 2004] also utilizes the equation in image matching. This basic concept is related to extraction of geometrical shape feature.

Topology optimization: The PDE based shape feature evaluation is proposed in topology optimization [Sato et al. 2017]. The

manufacturability in the molding process is evaluated by superposition of the solution of PDE. The main advantages are the shape and topological sensitivities derived by using the adjoint variable method and free from restriction of the design space in the optimization procedure.

3 CONCEPT AND OVERVIEW

The basic concept of shape features extraction by the linear partial differential equation (PDE) is a shape feature extracting method of target geometrical features, such as the thickness, skeleton, orientations and curvature, in the target image as a function of the solution of linear PDE system as shown in the Figure 1. This paper presents a formulation of a PDE system and functions for basic geometrical shape features represented by the solution of the PDE system.

The proposed method has the following advantages:

- (1) Multiple geometrical features are computed at once by solving the PDE system only. In particular, the computation with respect to distance is not required.
- (2) Relatively small shape fractionation on the surface is automatically neglected by the diffusion effect of the PDE. That is, the proposed method is automatically considering robustness.
- (3) The thickness extraction does not require any topological constraint and distinction of surfaces between inner and outer.
- (4) The basic concept and its mathematical formulation are not dependent on the structure of image data. Therefore, the formulation is effective for Stereolithography (STL), voxel and any other structures.
- (5) The formulation of PDE and geometrical shape feature functions are not dependent on the dimension.

4 FORMULATION

4.1 partial differential equation for shape features extraction

First of all, I define the PDE system for extraction of geometrical shape features in a binary image. I consider a reference domain Ω_R consisting of a black domain Ω and a white domain $\Omega_R \setminus \Omega$, whose digital signals are 1 and 0, respectively. I assume that the reference domain Ω_R is sufficiently huge to contain the image frame as shown in Figure 2. Here, the extraction of shape features of the black domain Ω is considered. I remark that the shape feature of the white domain can be also considered by the opposite signal situation. Here, I focus on the similarity of shape features in optimization of the periodic homogenization [Allaire and Yamada 2018], which is one method in the computational mechanics field. The PDE system is formulated as follows:

$$\begin{cases} -\operatorname{div}(\tilde{a}\nabla\chi_i - e_i\mathbf{1}_\Omega) + \alpha(1 - \mathbf{1}_\Omega)\chi_i = 0 & \text{in } \Omega_R \\ \chi_i = 0 & \text{on } \partial\Omega_R \end{cases} \quad (1)$$

where $\chi_i \in H^1(\Omega_R)$ are i -th state variables, e_i are the canonical bases of \mathbb{R}^d , $\tilde{a} > 0$ is the diffusion coefficient and α is the damping coefficient. The characteristic function $\mathbf{1}_\Omega \in L^\infty(\Omega_R)$ is defined as

$$\mathbf{1}_\Omega(\mathbf{x}) := \begin{cases} 1 & \text{for } \mathbf{x} \in \Omega \\ 0 & \text{for } \mathbf{x} \in \Omega_R \setminus \Omega. \end{cases} \quad (2)$$

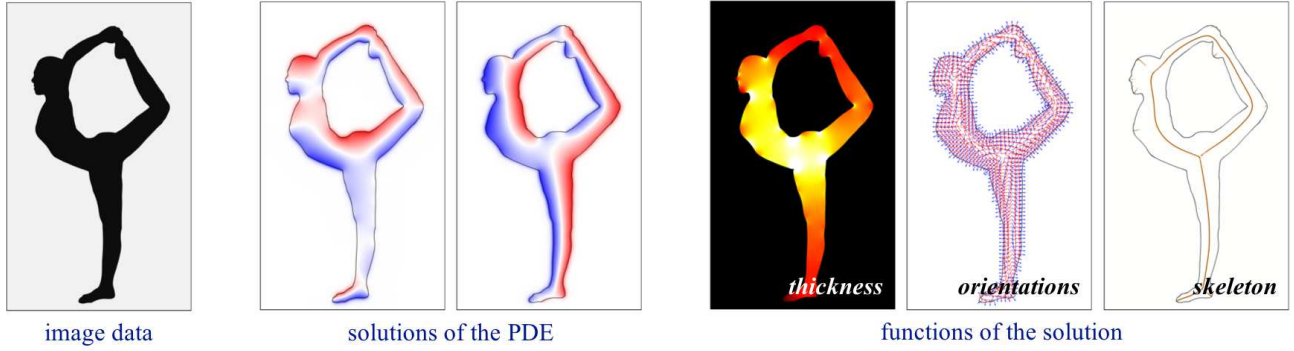


Fig. 1. An overview of my method: the proposed method extracts geometrical shape features, such as thickness, orientations and skeleton by the solutions of the proposed linear partial differential equation, whose coefficients are given by the image data. The left image represents the input image data to give the coefficients. The middle two images are solutions of the linear partial differential equation. The right three images are distribution values of functions of the solved solutions.

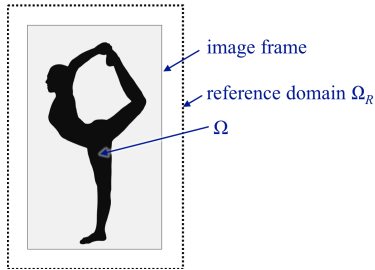


Fig. 2. Definitions for formulation

The characteristic function value is equivalent to binary data in the target image. I remark that surfaces do not have to be distinguished to inside or outside, because domains are distinguished by the characteristic function only in the same manner as the topology optimization method [Yamada et al. 2010]. Additionally, the proposed PDE does not have any topological restriction.

Next, I introduce a parameter a for the diffusion coefficient to be satisfied as $\tilde{a} := ah_0^2$ and characteristic length $h_0 > 0$ of the target shape size. I remark that concept of the characteristic length is the same the mechanics field. That is, the non-dimensional equation and the feature functions defined below are reasonable situations in general. Additionally, I set the damping coefficient α as follows:

$$\alpha := \frac{4}{a} \quad (3)$$

Then, the parameter of the proposed PDE is the non-dimensional diffusion parameter a only. The parameter a should be set sufficiently small, because the damping coefficient α set to keep off effects from the surrounding domain and boundary of the reference domain $\partial\Omega$. That is, the damping coefficient must be set to a large value to force the values of state variables χ_i into zero almost everywhere in the white domain. I remark that the details of formulation are found based on the author's intuition and trial and error approach. The most remarkable point is that the number of potential fields is equal to the dimension number. That is, the shape features

extraction is required for a vector field consisting of independent potential fields.

Next, we define the following tensor \mathbb{S}^* for extraction of key shape features.

$$\mathbb{S}_{ij}(\{\chi\}_{1 \leq i \leq d}) := \frac{1}{2} \left(\frac{\partial \chi_i}{\partial x_j} + \frac{\partial \chi_j}{\partial x_i} \right) \quad (4)$$

Here, I call the tensor \mathbb{S} 'shape feature tensor'. The key geometrical features are defined using the shape feature tensor \mathbb{S} . The eigen values $\lambda_s^{(i)}$ of the matrix respect the shape feature tensor and the normalized eigen vector $\mathbf{x}_s^{(i)}$, where I define the order of eigen values to satisfy $\lambda_s^{(i)} \leq \lambda_s^{(i+1)}$. Additionally, the base changed state variable $\tilde{\chi}_i$ using the eigen vector is defined as follows:

$$\begin{pmatrix} \tilde{\chi}_1 \\ \tilde{\chi}_2 \\ \vdots \\ \tilde{\chi}_d \end{pmatrix} := \begin{pmatrix} \mathbf{x}_s^1 & \mathbf{x}_s^2 & \cdots & \mathbf{x}_s^d \end{pmatrix}^T \begin{pmatrix} \chi_1 \\ \chi_2 \\ \vdots \\ \chi_d \end{pmatrix} \quad (5)$$

4.2 thickness function

The thickness is inversely proportional to the sum of the derivative of state variables in respect to each direction of the canonical base. That is, the following defined inverse thickness function f_h is inversely proportional to the local thickness in the target shape.

$$f_h(\{\chi\}_{1 \leq i \leq d}) := h_0^2 \left(\sum_{i=1}^d \frac{\partial \chi_i}{\partial x_i} \right) \mathbf{1}_\Omega \quad (6)$$

$$= h_0^2 \left(\sum_{i=1}^d \lambda_s^{(i)} \right) \mathbf{1}_\Omega \quad (7)$$

The detailed properties of the inverse thickness function f_h are discussed in Section 7. Using the property in respect to the thickness, the thickness function h_f is defined as follows:

$$h_f(\{\chi\}_{1 \leq i \leq d}) := h_0 \left\{ \frac{1}{f_h(\{\chi\}_{1 \leq i \leq d})} - a \right\} \mathbf{1}_\Omega. \quad (8)$$

The value of thickness function h_f represents local thickness of the black domain Ω . I remark that the function f_h is better than thickness function h_f in numerical evaluation such as its sensitivity, because a small denominator is required for an approximated evaluation.

4.3 orientation vector function

The state variable vector represents normal direction of the shape. The orientation in respect to normal direction is formulated as follows:

$$\mathbf{n}_f(\{\chi\}_{1 \leq i \leq d}) := \frac{1}{\sqrt{\sum_{i=1}^d \chi_i^2}} \begin{pmatrix} \chi_1 \\ \chi_2 \\ \vdots \\ \chi_d \end{pmatrix} \quad (9)$$

The tangential orientation vector \mathbf{t}_f is computed by rotational transformation of the normal orientation vector \mathbf{n}_f .

4.4 skeleton function

One of the skeleton functions is formulated as follows:

$$s_f(\{\chi\}_{1 \leq i \leq d}) := \mathcal{P}\left(\frac{\sqrt{\tilde{\chi}_1^2}}{\lambda_1}\right) \mathbf{1}_\Omega. \quad (10)$$

where \mathcal{P} is a pulse function defined as:

$$\mathcal{P}(x) = \begin{cases} 0 & \text{if } -w > x \\ 1 & \text{if } -w \leq x \leq w \\ 0 & \text{if } w < x \end{cases} \quad (11)$$

The parameter $w > 0$ for width of the non-zero value domain should be set to obtain the expected width such as pixel size. In three-dimensions, the function estimates the medial surfaces. Therefore, another function may be defined based on the requirements in each application.

5 NUMERICAL IMPLEMENTATION

The computational procedure is essentially the same as numerical analysis based on the finite element method such as stress analysis as follows:

- (1) The reference domain within target shape is defined. In general, the reference domain is set to surround input image data.
- (2) The reference domain is discretized finite elements whose material properties are defined based on the characteristic function $\mathbf{1}_\Omega$, which is defined by the input image data.
- (3) The PDE system (1) is solved using the finite element method. That is, the numerical solution of the state variables $\chi_i(\mathbf{x})$ are given.
- (4) The target geometrical shape feature is computed by the state variables $\chi_i(\mathbf{x})$.

It is easily implemented by using general finite element analysis software. In this paper, the numerical examples shown in Sections 7 and 8 are demonstrated using the commercial software 'COMSOL Multiphysics'. I remark that the boundary element method is also

useful to analyze the proposed PDE if an input data format is surface data such as STL data.

6 ANALYTICAL VALIDATION IN ONE DIMENSION

The analytical solutions of the proposed PDE is easily derived in one dimension. In order to validate the proposed method, therefore, a one dimensional case is considered. The distribution of black domain shown in Figure 3 is considered. That is, the black domain

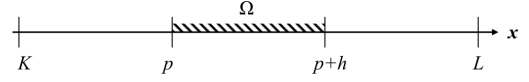


Fig. 3. an isolate domain in one-dimension

exists between $x = p$ and $x = p + h$. The governing equation and the boundary condition are

$$(\tilde{a}\chi')' + \alpha\chi = 0 \quad \text{if } K \leq x < p \quad (12)$$

$$(\tilde{a}\chi' - 1)' = 0 \quad \text{if } p \leq x \leq p + h \quad (13)$$

$$(\tilde{a}\chi')' + \alpha\chi = 0 \quad \text{if } p + h < x \leq L \quad (14)$$

$$\chi = 0 \quad \text{on } x = K \quad (15)$$

$$\chi = 0 \quad \text{on } x = L \quad (16)$$

Then, the analytical solution is derived as follows:

$$\chi(x) = \begin{cases} c_1 e^{\lambda x} + c_2 e^{-\lambda x} & \text{if } K \leq x < p \\ c_3 x + c_4 & \text{if } p \leq x \leq p + h \\ c_5 e^{\lambda x} + c_6 e^{-\lambda x} & \text{if } p + h < x \leq L \end{cases} \quad (17)$$

where λ is $\lambda = \sqrt{\alpha/\tilde{a}}$. Additionally, the thickness function $h_f(\chi)$ is as follows:

$$h_f(\chi) = \left(\frac{1}{h_0} \frac{1}{c_3} - h_0 a \right) \mathbf{1}_\Omega \quad (18)$$

The constants c_i are determined based on the boundary conditions (15) and (16), and continuous conditions in respect to state variable χ and the normal flux at $x = p$ and $x = p + h$:

$$\begin{aligned} c_1 &= -\frac{h}{\tilde{a}} \left(\frac{e^{\lambda(2L+p)} - e^{\lambda(3p+2h)}}{(2+\lambda h)e^{2\lambda(L+p)} + (\lambda h e^{2\lambda L} + (2-\lambda h)e^{2\lambda(p+h)})e^{2\lambda K} + \lambda h e^{2\lambda(2p+h)}} \right) \\ c_2 &= \frac{h e^{2\lambda K}}{\tilde{a}} \left(\frac{e^{\lambda(2L+p)} + e^{\lambda(3p+2h)}}{(2+\lambda h)e^{2\lambda(L+p)} + (\lambda h e^{2\lambda L} + (2-\lambda h)e^{2\lambda(p+h)})e^{2\lambda K} + \lambda h e^{2\lambda(2p+h)}} \right) \\ c_3 &= -\frac{2}{\tilde{a}} \left(\frac{e^{2\lambda(K+p+h)} - e^{2\lambda(L+p)}}{(2+\lambda h)e^{2\lambda(L+p)} + (\lambda h e^{2\lambda L} + (2-\lambda h)e^{2\lambda(p+h)})e^{2\lambda K} + \lambda h e^{2\lambda(2p+h)}} \right) \\ c_4 &= \frac{1}{\tilde{a}} \left(\frac{-(2p+h)e^{2\lambda(L+p)} + (h e^{2\lambda L} + (2p+h)e^{2\lambda(p+h)})e^{2\lambda K} - h e^{2\lambda(2p+h)}}{(2+\lambda h)e^{2\lambda(L+p)} + (\lambda h e^{2\lambda L} + (2-\lambda h)e^{2\lambda(p+h)})e^{2\lambda K} + \lambda h e^{2\lambda(2p+h)}} \right) \\ c_5 &= -\frac{h}{\tilde{a}} \left(\frac{e^{\lambda(2K+p+h)} + e^{\lambda(2p+h)}}{(2+\lambda h)e^{2\lambda(L+p)} + (\lambda h e^{2\lambda L} + (2-\lambda h)e^{2\lambda(p+h)})e^{2\lambda K} + \lambda h e^{2\lambda(2p+h)}} \right) \\ c_6 &= \frac{h}{\tilde{a}} \left(\frac{e^{\lambda(2L+2K+p+h)} + e^{\lambda(2L+3p+h)}}{(2+\lambda h)e^{2\lambda(L+p)} + (\lambda h e^{2\lambda L} + (2-\lambda h)e^{2\lambda(p+h)})e^{2\lambda K} + \lambda h e^{2\lambda(2p+h)}} \right) \end{aligned}$$

If the black domain is sufficiently far from the boundaries $x = K$ and $x = L$, then I obtain the following:

$$\begin{aligned} \lim_{\substack{K \rightarrow -\infty \\ L \rightarrow \infty}} c_1 &= -\frac{he^{-\lambda p}}{\tilde{a}(\lambda h + 2)} & \lim_{\substack{K \rightarrow -\infty \\ L \rightarrow \infty}} c_2 &= 0 & \lim_{\substack{K \rightarrow -\infty \\ L \rightarrow \infty}} c_3 &= \frac{2}{\tilde{a}(\lambda h + 2)} \\ \lim_{\substack{K \rightarrow -\infty \\ L \rightarrow \infty}} c_4 &= -\frac{2p + h}{\tilde{a}(\lambda h + 2)} & \lim_{\substack{K \rightarrow -\infty \\ L \rightarrow \infty}} c_5 &= 0 & \lim_{\substack{K \rightarrow -\infty \\ L \rightarrow \infty}} c_6 &= \frac{he^{\lambda(p+h)}}{\tilde{a}(\lambda h + 2)} \end{aligned}$$

Therefore, we obtain

$$\lim_{\substack{K \rightarrow -\infty \\ L \rightarrow \infty}} \chi(x) = \begin{cases} \frac{h}{\tilde{a}(\lambda h + 2)} e^{\lambda(x-p)} & \text{if } x < p \\ \frac{1}{\tilde{a}(\lambda h + 2)} (2x - (2p + h)) & \text{if } p \leq x \leq p + h \\ \frac{h}{\tilde{a}(\lambda h + 2)} e^{-\lambda(x-(p+h))} & \text{if } p + h < x \end{cases} \quad (19)$$

and

$$\lim_{\substack{K \rightarrow -\infty \\ L \rightarrow \infty}} h_f(\chi) = \begin{cases} 0 & \text{if } x < p \\ h & \text{if } p \leq x \leq p + h \\ 0 & \text{if } p + h < x \end{cases} \quad (20)$$

The value of the thickness function in the black domain is exactly equivalent to its thickness h , if the black domain sufficiently far from the boundaries of the reference domain. Therefore, the damping coefficient is set to a relatively huge value to satisfy the situation. If the black domain is relatively far from another black domain, the thickness function in the black domain is also exactly equivalent to its thickness h . This case is also confirmed by considering the periodic domain and taking the limit in respect to the period. Here, the most notable point is that thickness is extracted without any distance computation.

The orientation is not considered in a one dimensional case. The skeleton is defined without the base transformation in one dimension. Then, the skeleton obviously indicates a point at the center of the black domain, because the distribution of state variable $\chi(x)$ described in Equation (19) is zero at $x = p + \frac{h}{2}$.

Next, I demonstrate the analytical solution of the 1-dimensional case. The cases (a), (b) and (c) show effects on h , p and a , respectively. The parameters are shown in Table 1. As shown in Figure

Table 1. paramters in 1-dimensional computations

	K	L	h_0	h	p	a
case 1	0.0	1.0	0.2	–	0.2	0.2
case 2	0.0	1.0	0.2	0.2	–	0.2
case 3	0.0	1.0	0.2	0.2	0.4	–

4, the solution χ is exponentially damped in the white domain and a linear function in the black domain Ω . I confirmed that profile of the state variable χ is fixed when the parameter p is changed as shown in Figure 4(b). Therefore, a shape is equivalently evaluated to the shape whose position has been changed. Additionally, the effect from another shape or boundary is neglected when the damping coefficient is set to a relatively huge value. This is because

the distribution of the state variable χ is exponentially converged to zero in the white domain as shown in Figure 4(c). Therefore, I confirmed that the proposed method correctly evaluates the geometrical features in one dimension.

I remark that the characteristic length h_0 should be set to about the smallest target thickness, because the proposed method is not satisfied in a relatively small shape by the diffusion effect of the PDE. In other words, relatively small shape fractionation is neglected, because the diffusion term effects averaging the local information in the PDE system. Although the smaller diffusion coefficient gives more precise evaluation, a small diffusion coefficient is required for a fine finite element mesh in numerical computation. Therefore, the parameter a has to be set to satisfy the above discussed situation. Additionally, the finite element mesh size is determined by the value of parameter a .

7 NUMERICAL VALIDATION IN TWO DIMENSION

7.1 multiple bar shape

The two dimensional case shown in Figure 5 (a) is considered. As shown in the figure, the input image data includes multiple bars with respectively constant thickness, whose thicknesses h are set to 0.2, 0.25, 0.3, 0.35, 0.4, 0.45, 0.55 and 0.6, respectively. The image size is 5×8 . The parameters of the PDE are set to $h_0 = 0.3$ and $a = 0.2$.

The domain is discretized using the triangular elements and I use \mathbb{P}_2 finite elements whose maximal length is 0.05. Then, the obtained state variables χ_1 and χ_2 are shown in Figure 5 (d) and (e). Based on the solved state variables, the normal orientation vector $\mathbf{n}_f(\chi_1, \chi_2)$, the tangential orientation vector $\mathbf{t}_f(\chi_1, \chi_2)$, the inverse thickness function $f_h(\chi_1, \chi_2)$, the thickness function $h_f(\chi_1, \chi_2)$ and the skeleton function $s_f(\chi_1, \chi_2)$ are computed as shown in Figure 5.

First of all, the properties of inverse thickness function f_h are discussed. As shown in Figure 5(g), the values are constant in the black domain excluding around the corners. The relationship between each value of inverse thickness function f_h and thickness of the bar is plotted in Figure 5(h), which longitude and abscissa axis are the averaged value of $1/f_h$ and thickness of bar shapes, respectively. The averaged values are computed in each middle domain which width is 5 to avoid the corner effect. Additionally, the linear function estimated by the least squares method is also shown. The coefficient of determination in the estimation is $R^2 = 1.0000$. Therefore, I confirmed that the inverse thickness function f_h is inversely proportional to each thickness precisely. Figure 5(i) also represents the relationship between the value of the thickness function h_f and the thickness of each bar. The blue line represents the estimated linear function by the least squares method. The coefficient of determination in the estimation is also $R^2 = 1.0000$. Therefore, I confirmed that the thickness function f_h is proportional to each thickness precisely.

I remark that the linear function does not cross the origin. Although the local thickness is precisely estimated around the value of h_0 , the relative small thickness is excessively estimated. The effect is come from the diffusion term in the PDE. Therefore, I remark

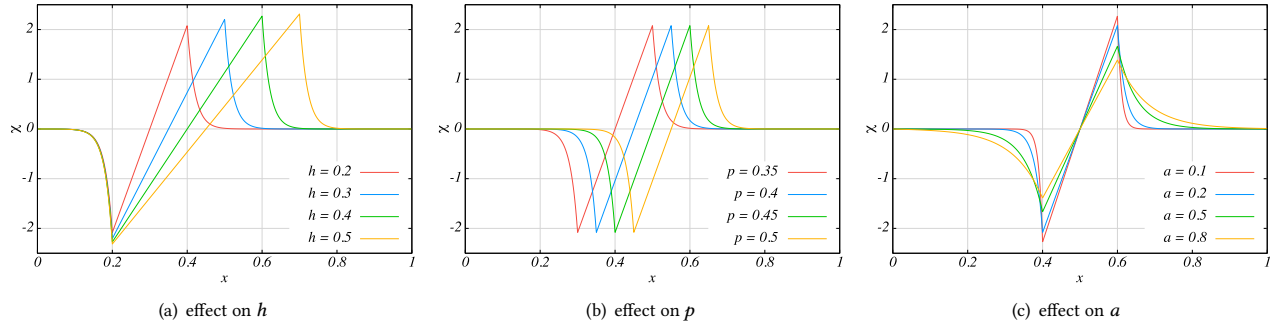


Fig. 4. Analytical solutions of the one dimensional case

again that the value of parameter h_0 should be set to target smallest thickness.

The value of thickness function h_f is equivalent to each thickness as shown in Figure 5(f). The skeleton shown in Figure 5(c) is also appropriately estimated because the curve is close to the definition of medial axis [Blum 1967]. The orientation vectors are also good estimation as shown in Figure 5(b).

7.2 complex shape by using the basic shapes

I examine the effectiveness of the proposed method in complex shape. The image size is set to 1×1 . The parameters of the PDE are set to $h_0 = 0.3$ and $a = 0.2$. The domain is discretized using the triangular elements and I use \mathbb{P}_2 finite elements.

To begin with, I consider an image including characteristic shapes as shown in Figure 6. Now, I focus on the ring shapes with respectively constant thicknesses located around the bottom side in the image. Therefore, the inverse thickness and thickness function values must be constant in each ring shape. I confirm that the requirement is satisfied and the expected magnitude relation among the values of thickness function h_f is also satisfied. Additionally, the orientation vector and the skeleton function indicate also appropriate features.

Second, I focus on the cubic shapes located around the upper left corner. Although each location and angle is different, the thickness function values are equivalent. Therefore, I confirmed that the dependency of these locations and angles are extremely low in the proposed method. Additionally, the orientation vectors and skeleton function indicate appropriate features. I note that the medial axes of the cubic shapes are its diagonal lines.

Next, I focus on the cross shape located around the center of the image. The intersection is cut out to provide constant thickness with diagonal directions. I confirmed that the thickness function value at the intersection is appropriate. That is, the thickness is equivalently evaluated to straight bars.

Finally, I focus on the full image. The shape and topology of the image are extremely complex. However, each shape features are appropriately extracted at the same time. That is, the proposed method does not have any topological constraint.

7.3 General shapes

I examine the effectiveness of the proposed method in general shapes. The image size is set to 1×1 in all examples. The parameters of PDE are set to $h_0 = 0.3$ and $a = 0.2$ for all of the following examples. The reference domain is discretized using the triangular elements and I use \mathbb{P}_2 finite elements. Here, I consider three types of general shape in two dimensions as shown in Figure 7, Figure 8 and Figure 9. As shown, the input images have complex geometrical features. The inverse thickness and thickness function values are globally appropriate as shown the figures. In the local point of view, sharply dented shapes are estimated as a thick shape. Additionally, a relatively small fluctuated shape is neglected, because the small feature is averaged by the diffusion effect in the PDE. The orientation vectors and skeleton are also globally appropriate. However, unconnected skeletons are obtained, because the proposed function is defined based on the concept of the medial axis and does not consider the connectivity. Therefore, different functions have to be considered when a connected skeleton is extracted.

8 NUMERICAL VALIDATION IN THREE DIMENSION

8.1 multiple box shape

I apply the proposed method to three dimensional cases. To begin with, the simple three dimensional case shown in Figure 10 (a) is considered. The box sizes are $0.7 \times 0.9 \times 0.1$, $0.7 \times 0.9 \times 0.15$ and $0.7 \times 0.9 \times 0.2$. Therefore, each thickness is 0.1, 0.15 and 0.2 excluding around the edges. The parameters of PDE are set to $h_0 = 0.1$ and $a = 0.2$. The domain is discretized using the tetrahedral elements and I use \mathbb{P}_2 finite elements.

As shown, the thickness function values indicate appropriate values. That is, I confirm that the thickness function h_f is effective in three dimensions. The obtained orientation vectors are also appropriate, because the orientation is equivalent to the normal direction of each surface. The orientation vector on the cross sectional surface as shown in Figure 10(c) is equivalent to the rectangle case in two dimensions. Additionally, I confirm that the skeleton function is equivalent to the medial surface. Therefore, the proposed method is effective in the simple three dimensional case.

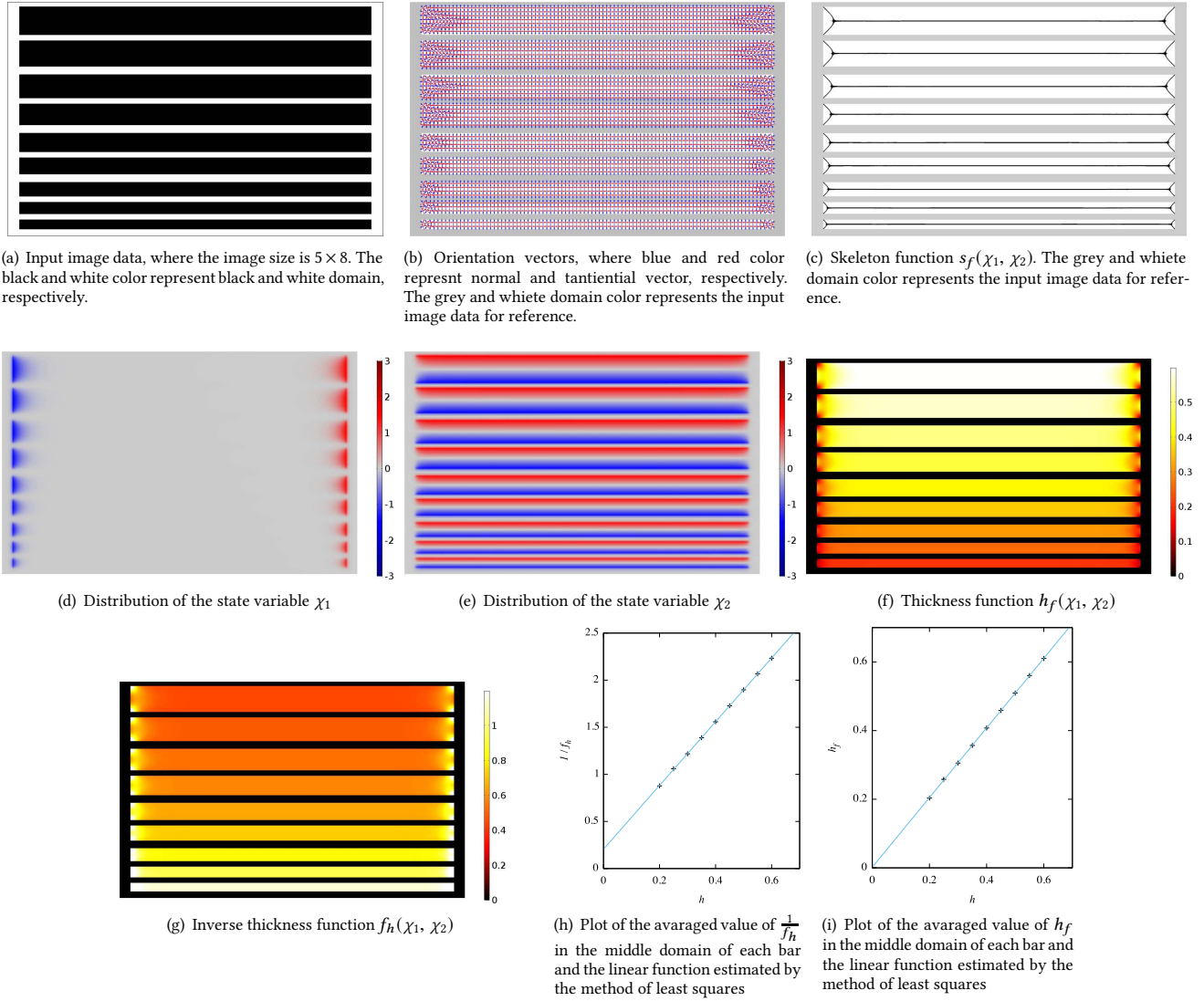


Fig. 5. Numerical results of a multiple bars image with different thickness

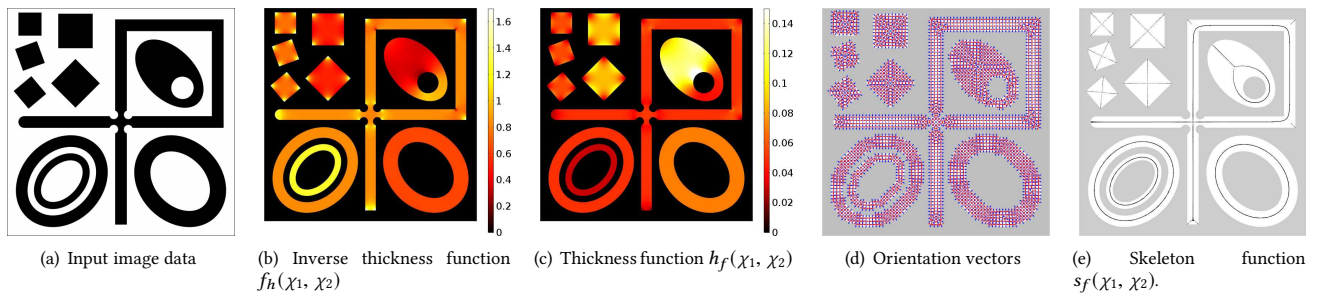


Fig. 6. A Numerical example of a two-dimensional complex shape

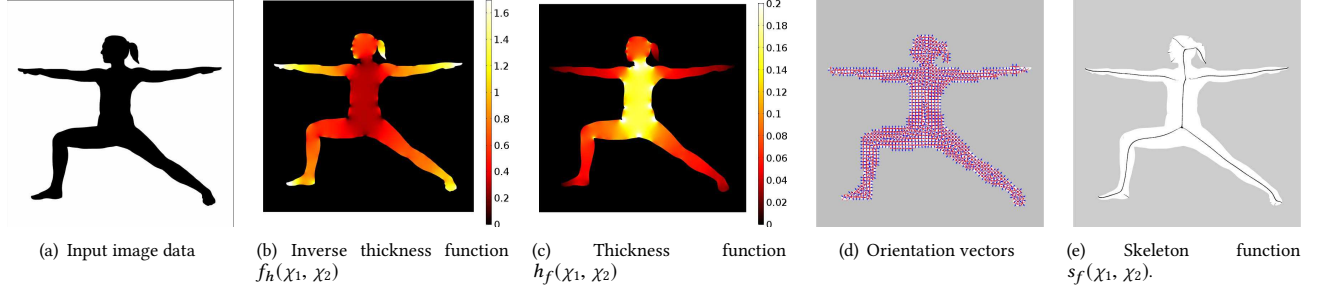


Fig. 7. Case 1 of general shape in two dimension

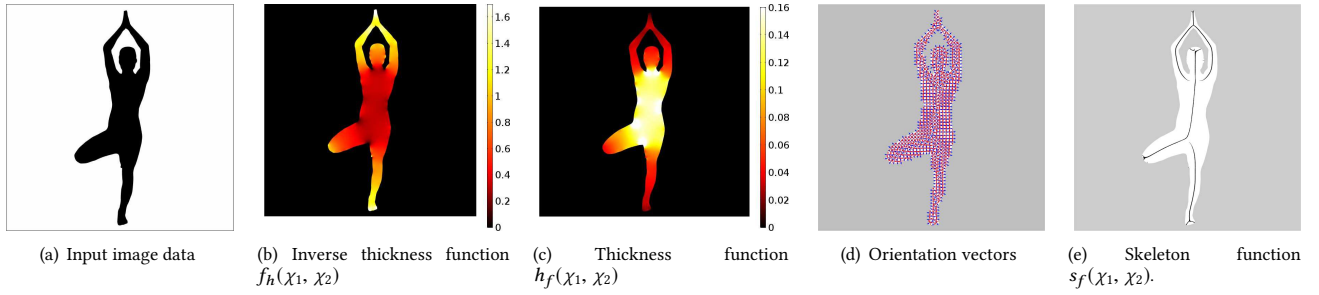


Fig. 8. Case 2 of general shape in two dimension

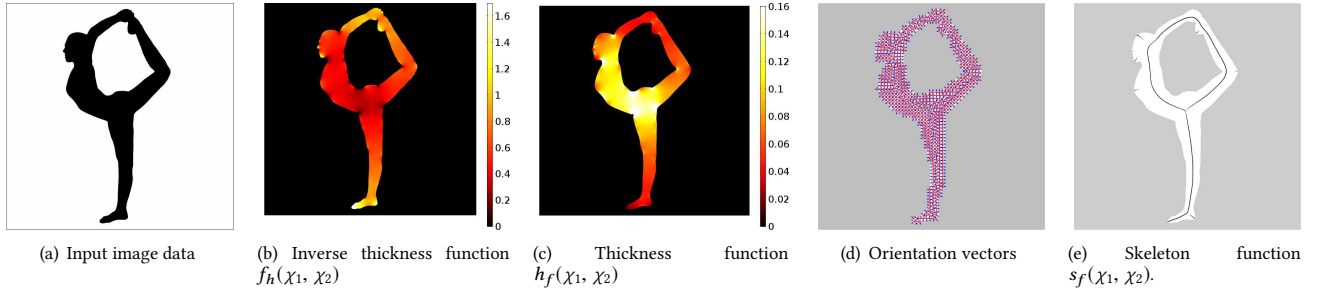


Fig. 9. Case 3 of general shape in two dimension

8.2 complex and general shapes

I examine the effectiveness of the proposed method in three dimensional general shapes. The parameters of PDE are set to $h_0 = 0.1$ and $a = 0.2$ for all of the following examples. The domain is discretized using the tetrahedral elements and I use \mathbb{P}_2 finite elements.

Figures 11, 12 and 13 provide numerical examples for topologically complex shapes. Especially, Figure 13 is a double Mobius band model. That is, the surfaces does not divided to inside and outside. As shown, the proposed method appropriately provides these geometrical features without any topological constraint. Additionally, the local thickness is computed without distinction between inner and outer surfaces.

Figures 14 and 15 provide shapes with relatively small fluctuation. As shown, these cases are also appropriately computed these geometrical features.

9 CONCLUSIONS AND FUTURE WORK

This paper presents a unified method of extraction for geometrical shape features by using the linear PDE. I achieved the following:

- (1) The linear PDE for extraction of the geometrical features was formulated.
- (2) The functions for orientation vector, inverse thickness, thickness and skeleton were formulated by the solutions of the proposed PDE.

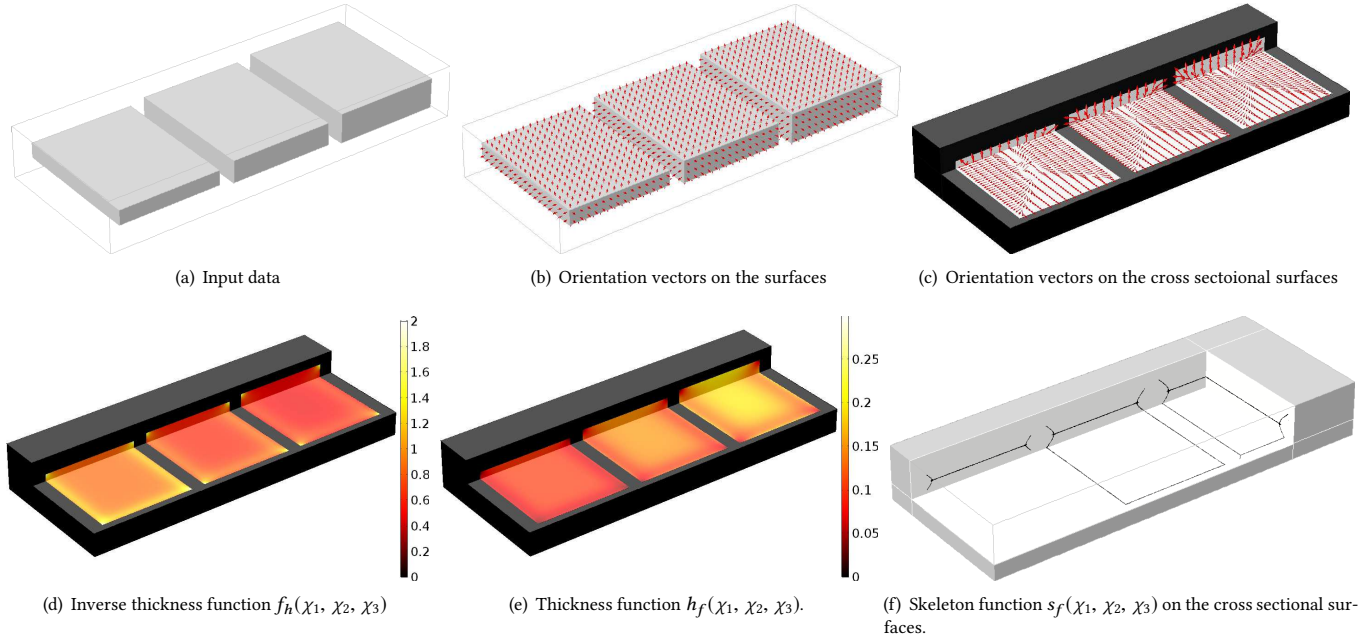


Fig. 10. Box shapes with different thicknesses

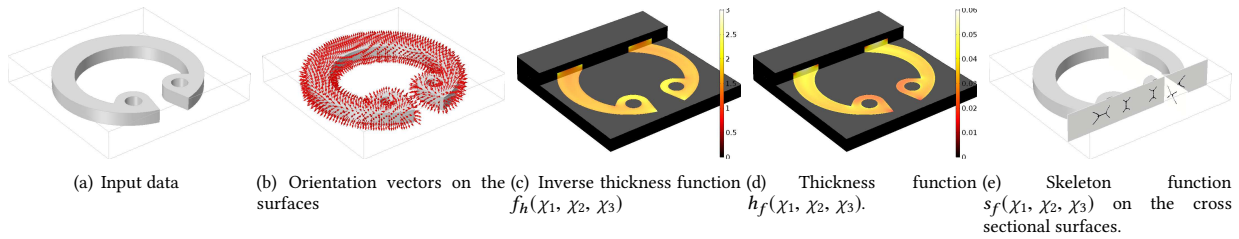


Fig. 11. C-type ring

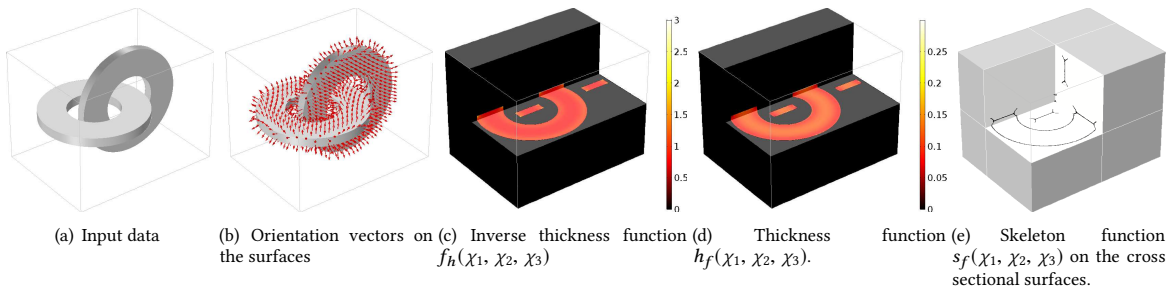


Fig. 12. Crossed rings

(3) The analytical solution was derived in the one dimensional case. Based on the derived solution, validity of the proposed function was confirmed.

(4) Several numerical examples were provided to confirm the usefulness of the proposed method for the various geometrical shape features examined in this paper. Additionally, I confirmed that these geometrical shape features were extracted without any topological constraint.

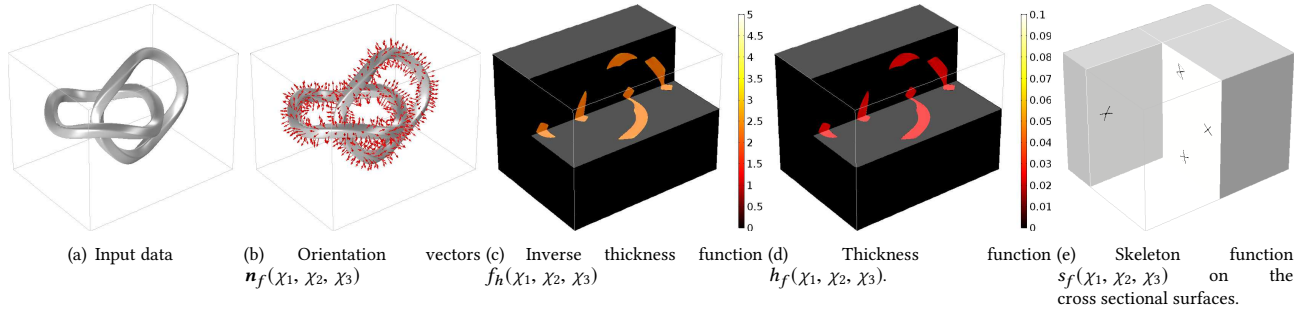


Fig. 13. Double Mobius band model

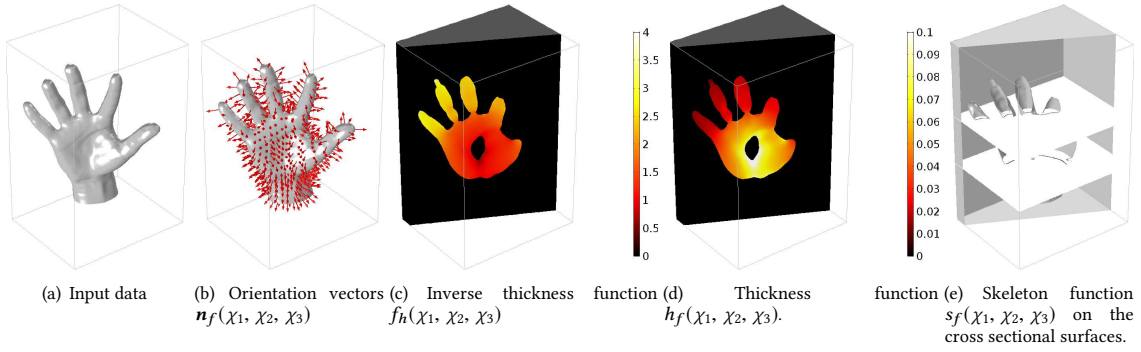


Fig. 14. Arm model

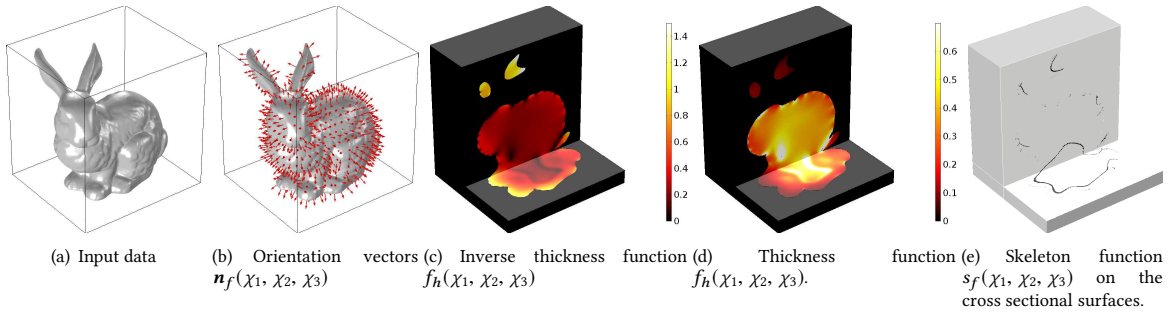


Fig. 15. The Stanford bunny model

In the future, functions for other geometrical features, such as curve-skeleton, will be considered. Additionally, the formulation will be extended to gray images for wider applications.

ACKNOWLEDGMENTS

The author acknowledges comments of Professor Grégoire Allaire (École Polytechnique) in the validation of the proposed model.

REFERENCES

G. H. Abdel-Hamid and Yee-Hong Yang. 1994. Multiresolution Skeletonization an Electrostatic Field-based Approach. In *Proceedings of 1st International Conference on Image Processing*, Vol. 1. IEEE, 949–953. <https://doi.org/10.1109/ICIP.1994.413249>

- Oscar Acosta, Pierrick Bourgeat, Maria A Zuluaga, Jurgen Frapp, Olivier Salvado, and Sébastien Ourselin. 2009. Automated Voxel-Based 3D Cortical Thickness Measurement in a Combined Lagrangian-Eulerian PDE approach Using Partial Volume Maps. *Medical Image Analysis* 13, 5 (2009), 730–743. <https://doi.org/10.1016/j.media.2009.07.003>
- Iman Aganj, Guillermo Sapiro, Neelroop Parikhshak, Sarah K Madsen, and Paul M Thompson. 2009. Measurement of Cortical Thickness from MRI by Minimum Line Integrals on Soft-Classified Tissue. *Human Brain Mapping* 30, 10 (2009), 3188–3199. <https://doi.org/10.1002/hbm.20740>
- Narendra Ahuja and Jen-Hui Chuang. 1997. Shape Representation Using a Generalized Potential Field Model. *IEEE Transactions on Pattern Analysis and Machine Intelligence* 19, 2 (1997), 169–176. <https://doi.org/10.1109/34.574801>
- Grégoire Allaire and Takayuki Yamada. 2018. Optimization of Dispersive Coefficients in the Homogenization of the Wave Equation in Periodic Structures. *Numer. Math.* in press, - (2018), -. <https://doi.org/10.1007/s00211-018-0972-4>

- Nina Amenta, Sunghee Choi, and Ravi Krishna Kolluri. 2001. The Power Crust, Unions of Balls, And the Medial Axis Transform. *Computational Geometry* 19, 2-3 (2001), 127–153. [https://doi.org/10.1016/S0925-7721\(01\)00017-7](https://doi.org/10.1016/S0925-7721(01)00017-7)
- Fernanda A Andaló, Paulo AV Miranda, R da S Torres, and Alexandre X Falcão. 2010. Shape Feature Extraction And Description Based on Tensor Scale. *Pattern Recognition* 43, 1 (2010), 26–36. <https://doi.org/10.1016/j.patcog.2009.06.012>
- Carlo Arcelli, Gabriella Sanniti di Baja, and Luca Serino. 2011. Distance-Driven Skeletonization in Voxel Images. *IEEE Transactions on Pattern Analysis and Machine Intelligence* 33, 4 (2011), 709–720. <https://doi.org/10.1109/TPAMI.2010.140>
- Pal Benko, Ralph R. Martin, and Tamas Varady. 2001. Algorithms for Reverse Engineering Boundary Representation Models. *Computer-Aided Design* 33, 11 (2001), 839–851. [https://doi.org/doi.org/10.1016/S0010-4485\(01\)00100-2](https://doi.org/doi.org/10.1016/S0010-4485(01)00100-2)
- Ingmar Bitter, Arie E. Kaufman, and Mie Sato. 2001. Penalized-Distance Volumetric Skeleton Algorithm. *IEEE Transactions on Visualization and Computer Graphics* 7, 3 (2001), 195–206. <https://doi.org/10.1109/2945.942688>
- Harry Blum. 1967. A Transformation for Extracting New Descriptors of Shape. *Models for Perception of Speech and Visual Forms* (1967), 362–380.
- Harry Blum and Roger N Nagel. 1978. Shape Description Using Weighted Symmetric Axis Features. *Pattern Recognition* 10, 3 (1978), 167–180. [https://doi.org/10.1016/0031-3203\(78\)90025-0](https://doi.org/10.1016/0031-3203(78)90025-0)
- M Jorge Cardoso, Matthew J Clarkson, Marc Modat, and Sebastien Ourselin. 2011. On the Extraction of Topologically Correct Thickness Measurements Using Khalimsky's Cubic Complex. In *Biennial International Conference on Information Processing in Medical Imaging*. Springer, 159–170. https://doi.org/10.1007/978-3-642-22092-0_14
- Matthew J Clarkson, M Jorge Cardoso, Gerard R Ridgway, Marc Modat, Kelvin K Leung, Jonathan D Rohrer, Nick C Fox, and Sébastien Ourselin. 2011. A Comparison of Voxel And Surface Based Cortical Thickness Estimation Methods. *Neuroimage* 57, 3 (2011), 856–865. <https://doi.org/10.1016/j.neuroimage.2011.05.053>
- Nicu D Cornea, Deborah Silver, and Patrick Min. 2007. Curve-Skeleton Properties, Applications, and Algorithms. *IEEE Transactions on Visualization And Computer Graphics* 13, 3 (2007), 0530–548. <https://doi.org/10.1109/TVCG.2007.1002>
- Sandhitsu R Das, Brian B Avants, Murray Grossman, and James C Gee. 2009. Registration based Cortical Thickness Measurement. *Neuroimage* 45, 3 (2009), 867–879. <https://doi.org/10.1016/j.neuroimage.2008.12.016>
- Christos Davatzikos and N Bryan. 1996. Using a Deformable Surface Model to Obtain a Shape Representation of the Cortex. *IEEE Transactions on Medical Imaging* 15, 6 (1996), 785–795. <https://doi.org/10.1109/42.544496>
- Tomoyuki Fujimori and Hiromasa Suzuki. 2005. Surface Extraction from Multi-Material CT Data. In *Ninth International Conference on Computer Aided Design and Computer Graphics*. IEEE, 6. <https://doi.org/10.1109/CAD-CG.2005.79>
- Tanya Grigorishin, Gamal Abdel-Hamid, and Y-H Yang. 1998. Skeletonisation: An Electrostatic Field-Based Approach. *Pattern Analysis and Applications* 1, 3 (1998), 163–177. <https://doi.org/10.1007/BF01259366>
- Xiao Han, Dzung L Pham, Duygu Tosun, Maryam E Rettmann, Chenyang Xu, and Jerry L Prince. 2004. CRUISE: Cortical Reconstruction Using Implicit Surface Evolution. *NeuroImage* 23, 3 (2004), 997–1012. <https://doi.org/10.1016/j.neuroimage.2004.06.043>
- Tor Hildebrand and Peter Rüeggesser. 1997. A New Method for the Model-Independent Assessment of Thickness in Three-Dimensional Images. *Journal of Microscopy* 185, 1 (1997), 67–75. <https://doi.org/10.1046/j.1365-2818.1997.1340694.x>
- Chloe Hutton, Enrico De Vita, John Ashburner, Ralf Deichmann, and Robert Turner. 2008. Voxel-based Cortical Thickness Measurements in MRI. *Neuroimage* 40, 4 (2008), 1701–1710. <https://doi.org/10.1016/j.neuroimage.2008.01.027>
- Stephen E Jones, Bradley R Buchbinder, and Itzhak Aharon. 2000. Three-Dimensional Mapping of Cortical Thickness Using Laplace's Equation. *Human Brain Mapping* 11, 1 (2000), 12–32.
- Yinxiao Liu, Dakai Jin, Cheng Li, Kathleen F Janz, Trudy L Burns, James C Torner, Steven M Levy, and Punam K Saha. 2014. A Robust Algorithm for Thickness Computation at Low Resolution And Its Application to in Vivo Trabecular Bone CT Imaging. *IEEE Transactions on Biomedical Engineering* 61, 7 (2014), 2057–2069. <https://doi.org/10.1109/TBME.2014.2313564>
- Gabriele Lohmann, Christoph Preul, and Margret Hund-Georgiadis. 2003. Morphology-Based Cortical Thickness Estimation. In *Biennial International Conference on Information Processing in Medical Imaging*. Springer, 89–100. https://doi.org/10.1007/978-3-540-45087-0_8
- Ugo Montanari. 1968. A Method for Obtaining Skeletons Using a Quasi-Euclidean Distance. *Journal of the ACM* 15, 4 (1968), 600–624. <https://doi.org/10.1145/321479.321486>
- Kálmán Palágyi and Attila Kuba. 1998. A 3D 6-Subiteration Thinning Algorithm for Extracting Medial Lines. *Pattern Recognition Letters* 19, 7 (1998), 613–627. [https://doi.org/10.1016/S0167-8655\(98\)00031-2](https://doi.org/10.1016/S0167-8655(98)00031-2)
- Patrick Pérez, Michel Gangnet, and Andrew Blake. 2003. Poisson image editing. *ACM Transactions on Graphics* 22, 3 (2003), 313–318. <https://doi.org/10.1145/1201775.882269>
- Kelvin R Rocha, Anthony J Yezzi, and Jerry L Prince. 2005. A Hybrid Eulerian-Lagrangian Approach for Thickness, Correspondence, And Gridding of Annular Tissues. In *International Workshop on Computer Vision for Biomedical Image Applications*. Springer, 72–81.
- Punam Kumar Saha. 2005. Tensor Scale: A Local Morphometric Parameter with Applications to Computer Vision And Image Processing. *Computer Vision and Image Understanding* 99, 3 (2005), 384–413. <https://doi.org/10.1016/j.cviu.2005.03.003>
- Punam K Saha, Bidyut Baran Chaudhuri, and D Dutta Majumder. 1997. A New Shape Preserving Parallel Thinning Algorithm For 3D Digital Images. *Pattern Recognition* 30, 12 (1997), 1939–1955. [https://doi.org/10.1016/S0031-3203\(97\)00016-2](https://doi.org/10.1016/S0031-3203(97)00016-2)
- Punam K Saha and Felix W Wehrli. 2004. Measurement of Trabecular Bone Thickness in the Limited Resolution Regime of in vivo MRI by Fuzzy Distance Transform. *IEEE Transactions on Medical Imaging* 23, 1 (2004), 53–62. <https://doi.org/10.1109/TMI.2003.819925>
- Punam K Saha, Felix W Wehrli, and Bryon R Gomberg. 2002. Fuzzy Distance Transform: Theory, Algorithms, And Applications. *Computer Vision and Image Understanding* 86, 3 (2002), 171–190. <https://doi.org/10.1006/cviu.2002.0974>
- Yuki Sato, Takayuki Yamada, Kazuhiro Izui, and Shinji Nishiwaki. 2017. Manufacturability Evaluation for Molded Parts Using Fictitious Physical Models, And Its Application in Topology Optimization. *The International Journal of Advanced Manufacturing Technology* 92, 1-4 (2017), 1391–1409. <https://doi.org/10.1007/s00170-017-0218-0>
- Marietta LJ Scott, Paul A Bromiley, Neil A Thacker, CE Hutchinson, and Alan Jackson. 2009. A Fast, Model-Independent Method for Cerebral Cortical Thickness Estimation Using MRI. *Medical Image Analysis* 13, 2 (2009), 269–285. <https://doi.org/10.1016/j.media.2008.10.006>
- Toshihiro Sera, Hideki Fujioka, Hideo Yokota, Akitake Makinouchi, Ryutaro Himeno, Robert C Schroter, and Kazuo Tanishita. 2003. Three-Dimensional Visualization and Morphometry of Small Airways From Microfocal X-Ray Computed Tomography. *Journal of biomechanics* 36, 11 (2003), 1587–1594. [https://doi.org/10.1016/S0021-9290\(03\)00179-9](https://doi.org/10.1016/S0021-9290(03)00179-9)
- Jian Sun, Jiaya Jia, Chi-Keung Tang, and Heung-Yeung Shum. 2004. Poisson Matting. In *ACM Transactions on Graphics*, Vol. 23. 315–321. <https://doi.org/10.1145/1186562.1015721>
- Takayuki Yamada, Kazuhiro Izui, Shinji Nishiwaki, and Akihiro Takezawa. 2010. A Topology Optimization Method Based on the Level Set Method Incorporating a Fictitious Interface Energy. *Computer Methods in Applied Mechanics and Engineering* 199, 45 (2010), 2876–2891. <https://doi.org/10.1016/j.cma.2010.05.013>
- Norio Yamashita, Shin Yoshizawa, and Hideo Yokota. 2014. Volume-Based Shape Analysis for Internal Microstructure of Steels. In *2014 IEEE International Conference on Image Processing*. IEEE, 4887–4891. <https://doi.org/10.1109/ICIP.2014.7025990>
- Yajie Yan, Kyle Sykes, Erin Chambers, David Letscher, and Tao Ju. 2016. Erosion Thickness on Medial Axes of 3D Shapes. *ACM Transactions on Graphics* 35, 4 (2016), 38. <https://doi.org/10.1145/2897824.2925938>
- Anthony Yezzi and Jerry L Prince. 2001. A PDE Approach for Measuring Tissue Thickness. In *Proceedings of the 2001 IEEE Computer Society Conference on Computer Vision and Pattern Recognition*, Vol. 1. IEEE. <https://doi.org/10.1109/CVPR.2001.990460>
- Anthony J Yezzi and Jerry L Prince. 2003. An Eulerian PDE approach for computing tissue thickness. *IEEE Transactions on Medical Imaging* 22, 10 (2003), 1332–1339. <https://doi.org/10.1109/TMI.2003.817775>
- Miao Zhenjiang. 2000. Zernike Moment-based Image Shape Analysis And Its Application. *Pattern Recognition Letters* 21, 2 (2000), 169–177. [https://doi.org/10.1016/S0167-8655\(99\)00144-0](https://doi.org/10.1016/S0167-8655(99)00144-0)

Received June 2018